J. Cell. Mol. Med. Vol 12, No 2, 2008 pp. 537-552

Researching into the cellular shape, volume and elasticity of mesenchymal stem cells, osteoblasts and osteosarcoma cells by atomic force microscopy

Denitsa Docheva [a], Daniela Padula [a, b], Cvetan Popov [a], Wolf Mutschler [a], Hauke Clausen-Schaumann [b, c], Matthias Schieker [a, *]

[a] *Experimental Surgery and Regenerative Medicine, Department of Surgery, Ludwig-Maximilians-University (LMU), Munich, Germany*

[b] *Precision- and Micro-Engineering, Engineering Physics, Faculty 06, Munich University of Applied Sciences, Munich, Germany*

[c] *Center for NanoScience (CeNS), Ludwig-Maximilians-University (LMU), Munich, Germany*

Received: July 26, 2007; Accepted: October 3, 2007

Abstract

Within the bone lie several different cell types, including osteoblasts (OBs) and mesenchymal stem cells (MSCs). The MSCs are ideal targets for regenerative medicine of bone due to their differentiation potential towards OBs. Human MSCs exhibit two distinct morphologies: rapidly self-renewing cells (RS) and flat cells (FC) with very low proliferation rates. Another cell type found in pathological bone conditions is osteosarcoma. In this study, we compared the topographic and morphometric features of RS and FC cells, human OBs and MG63 osteosarcoma cells by atomic force microscopy (AFM). The results demonstrated clear differences: FC and hOB cells showed similar ruffled topography, whereas RS and MG63 cells exhibited smoother surfaces. Furthermore, we investigated how selected substrates influence cell morphometry. We found that RS and MG63 cells were flatter on fibrous substrates such as polystyrene and collagen I, but much more rounded on glass, the smoothest surface. In contrast, cells with large area, namely FC and hOB cells, did not exhibit pronounced changes in flatness with regards to the different substrates. They were, however, remarkably flatter in comparison to RS and MG63 cells. We could explain the differences in flatness by the extent of adhesion. Indeed, FC and hOB cells showed much higher content of focal adhesions. Finally, we used the AFM to determine the cellular Young's modulus. RS, FC and hOB cells showed comparable stiffness on the three different substrates, while MG63 cells demonstrated the unique feature of increased elasticity on collagen I. In summary, our results show, for the first time, a direct comparison between the morphometric and biophysical features of different human cell types derived from normal and pathological bone. Our study manifests the opinion that along with RNA, proteomic and functional research, morphological and biomechanical characterization of cells also reveals novel cell features and interrelationships.

Keywords: bone • mesenchymal stem cells (MSCs) • osteoblasts (OBs) • osteosarcoma • atomic force microscopy (AFM) • Young's modulus • cytoskeleton • focal adhesion

Introduction

Osteoblasts (OBs) are bone forming cells which, during developmental and regenerative processes, descend from mesenchymal stem cells (MSCs) [1]. MSCs are plastic-adherent cells isolated from bone marrow or other tissues which possess self-renewal and multi-lineage differentiation capacities and therefore are potential candidates for cell-based clinical applications [2–4]. Upon treatment in culture, MSCs commence the transition to the OB lineage as they upregulate typical osteogenic markers and deposit a mineralized matrix [5]. However, in the described

*Correspondence to: Matthias SCHIEKER, MD, Experimental Surgery and Regenerative Medicine, Department of Surgery, Ludwig-Maximilians-University Munich, Nussbaumstr. 20, D-80336 Munich, Germany.
Tel.: +49 89 5160 7589
Fax: +49 89 5160 5482
E-mail: Matthias.Schieker@med.uni-muenchen.de

doi: 10.1111/j.1582-4934.2007.00138.x

experimental model not all MSCs within a given population differentiate into OBs. In addition, MSC cultures exhibit a high degree of heterogeneity with regard to their morphological appearance and capacity for replication. A series of reports from the Prockop group [6–10] have shown that MSCs can be assigned to at least two morphological types: rapidly self-renewing, small, round or spindle-shaped cells (RS cells) and slowly replicating, large, cuboidal or flattened cells (mature MSCs or FC cells as indicated here) [9]. Furthermore, RS cells manifested the highest multipotentiality. In brief, these observations suggest that the heterogeneity of MSC cultures may reflect different mesenchymal progenitors and RS cells may constitute the earliest precursors [11]. Another intriguing suggestion is that MSCs may be the cells of origin not only for 'normal' but also for 'pathological' OBs, for instance osteosarcoma cells [12, 13]. Osteosarcoma is the most common malignant bone tumour, which frequently arises within the metaphyseal growth plates, where MSCs concentrate, proliferate and differentiate. Furthermore, osteosarcoma is characterized by a spectrum of histopathologic subtypes depending on the predominant mesenchymal tissue represented. In particular, osteogenic osteosarcoma is composed of immature bone progenitors that produce abundant, amorphous osteoid lacking the characteristics of mature bone [14, 15]. Altogether, there are plenty of intimate, entwisted connections between MSCs, OBs and osteosarcoma cells, which need to be further explored. Our group has already been engaged in several studies researching the differences in protein expression between human MSCs (hMSCs), human OBs (hOBs) and osteosarcoma cell lines [16–18]. Here, we chose an alternative approach, which focuses, not on the biochemical properties of these cells, but on their structural and mechanical attributes. Mechanical properties, such as cytoskeleton organization, elasticity, membrane tension, cell shape and adhesion strength play an important role in cell fate and differentiation [19]. For example, dynamic arrangement of the actin network is critical in supporting the osteogenic differentiation of MSCs [20]. Additionally, MSC commitment to adipogenic or osteogenic lineages can be regulated *via* cell shape, cytoskeleton tension and endogenous Rho GTPase activity [21]. These studies demonstrate the importance of the mechanical characterization of cells. A feasible tool for performing such measurements is the atomic force microscope (AFM). The AFM technique is based on an ultra-sharp tip attached to a flexible cantilever spring, as well as accurate piezoactuators. Scanning the tip across the sample surface provides high-resolution topographic images, and even more *via* detecting the degree of the tip's deflection, the elasticity (Young's modulus) of the sample can be quantified. In recent years AFM has been used in numerous biological applications. AFM is an indispensable tool to study mechanical properties of bio-molecules. Thus, detailed insights into DNA mechanics, protein folding pathways, receptor-ligand pairs and molecular motors have been obtained (reviewed in Clausen-Schaumann *et al*. [22] and Engel and Muller [23]). In terms of cell biomechanics, AFM has also been used in variety of experimental set ups (reviewed Santos and Castanho [24]), from cell elastic characterization ([25] and reviewed in Costa [26]) to more functional analyses such as measuring the force of cell-cell adhesion and furrow stiffening of dividing cells ([27, 28] and reviewed in Simon and Durrieu [29]).

In the present study, we used AFM to search for differences in cell shape, volume and elasticity of hMSCs (RS cells and FC cells), hOBs and osteosarcoma cells (MG63 cell line). Moreover, we investigated if the morphometric and elastic properties of the cells are influenced by the substrates on which they are cultured (polystyrene, glass and collagen I). Finally, we looked for a link between the above characteristics, the actin organization and the adhesive profile of the chosen cells.

Material and methods

Cell culture

HMSCs were isolated from bone marrow by ficoll gradient centrifugation and purchased from Lonza (Verviers, Belgium). HMSCs were cultured in MEM Alpha GlutaMAX^{TM} culture media (Invitrogen, Karlsruhe, Germany) supplemented with 10% FBS (Sigma-Aldrich, Munich, Germany). HOBs were purchased from PromoCell (Heidelberg, Germany) and cultured according to the supplier's recommendations. These cells were originally isolated from human trabecular bone obtained during hip replacements. The MG63 cell line was derived from human bone osteosarcoma (ATCC, Wesel, Germany). MG63 cells were grown in DMEM (PAA, Pasching, Austria) containing 10% FBS. During routine culture, the cells where maintained

at 60–80% confluence in T75 culture flasks (Nunc, Wiesbaden, Germany), at 37°C in 5% CO_2. HMSCs and hOBs in 5–9 passage and MG63 cells in 5–13 passage were used in experiments.

Proliferation rate

During the expansion of hMSC, hOB and MG63 cells were detached by trypsin/EDTA (PAA) and counted using a haemocytometer (Brand, Wertheim, Germany). Population doubling (PD) and PD time were calculated according to Huang *et al.* [30], as counts from three passages were used.

Sample preparation

A total of 700–1000 cells/cm^2 were seeded on polystyrene (BD Falcon, Heidelberg) and on non- or collagen I-coated glass slides (Nunc), or Petri dishes (Schott, Mainz, Germany). For coating, 10 µg/ml collagen I (Upstate-Millipore, Dundee, UK) was laid on the glasses for 12 hrs at 4°C. Cells were let to attach on three different substrates for a minimum of 12 hrs. Prior to AFM scanning, the cells were fixed with 4% paraformaldehyde, rinsed with PBS and thereafter the slides were mounted on the microscope. AFM elasticity measurements were performed on live cells, therefore the culture media was supplemented with 25 mM HEPES (Sigma-Aldrich) and the Petri dishes were mounted on a heated microscope table (37°C). Altogether, 98 cells were used for the acquisition of high-resolution topographic images and elasticity measurements.

Atomic force microscopy

All AFM measurements were carried out using a NanoWizard AFM (JPK Instruments, Berlin, Germany), which was mounted on a modified microscope stage of an inverted optical microscope (Axiovert 200, Carl Zeiss, MicroImaging, Gottingen, Germany). The AFM had a maximum horizontal scanning range of 100 × 100 µm^2, and a vertical range of 15 µm. The optical microscope was used to select the desired cell, and to position the AFM tip. Silicone nitride cantilevers (MLCT-Microlever Probes, Veeco Instruments, Mannheim, Germany) with force constants around 20 mN/m were used. The force constants of all cantilevers were determined individually using the thermal noise method [31]. All AFM images were obtained in contact mode in liquid. Bare substrate surfaces were imaged with 512 × 512 pixels^2 at line rates of 5 Hz. Fixed cells were imaged with 1024 × 1024 pixels^2 at line rates of approximately 0.3–0.5 Hz and live cells were imaged with 512 × 512 pixels^2 at line rates of 0.7 Hz. Prior to acquisition of force *versus* indentation profiles, cells were imaged with the AFM.

For surface roughness analysis of bare substrates, 10 × 10 µm^2 AFM images (10 independent scans) were obtained and the mean height deviation from the principal x–y-plane $\langle \Delta H \rangle$ was calculated according to: $\langle \Delta \mathrm{H} \rangle = \frac{1}{\Delta x \Delta y} \int_{\Delta y} \int_{\Delta x} |\Delta H(x,y)| \, dxdy$, with $\Delta x = \Delta y = 10$ µm.

For morphometric analysis, several partial AFM images had to be acquired for cells larger than 100 × 100 µm^2. After subtracting the background plane, the partial cell images were stitched together using a home-made template matching algorithm which maximizes the normalized correlation coefficient of overlapping image parts [32]. AFM images of entire cells were then used to calculate cell length (l) (the longest diameter), width (w) (the diameter perpendicular to l), height (h) (the highest elevation), cross-sectional area (A) and volume (V). To perform quantitative comparison of cell shapes, geometrical form factors were calculated. The ellipse shape factor $s_1 = w/l$ describes the tendency of a cell to be long and narrow with $s_1 = 1$ for a disk-shaped cell and $s_1 \rightarrow \infty$ for a rod-shaped cell. The flatness shape factor $s_2 = h \cdot \sqrt{\pi/(4A)}$ simultaneously provides information about the cell area and height, and assumes the value $s_2 = 0$ for flat disks and $s_2 = 1$ for spherical ellipsoids [33, 34].

Elasticity measurements

The Young's modules of the cells were derived from force *versus* indentation profiles, which were acquired at 10 different points in the nuclear and peri-nuclear region of the cells (schematic model in Fig. 6A). The force-indentation-profiles were recorded at 0.7 Hz and to eliminate hydrodynamic effects, averages of trace and retrace were used. The Young's modules (E) were extracted from the above profiles by using a modified Hertz model [35, 36]. The model relates the loading force (F) of an indenting cone to the indentation (δ), *via* E, the Poisson ratio (ν) and the opening angle of the cone (α): $F = 2E \cdot \delta^2 \cdot \tan(\alpha)/(\pi[1-\nu^2])$ Replacing F by $k_c d$ and d by z-d, where k_c is the force constant and d the deflection one obtains: $z - z_0 = d - d_0 + \sqrt{\pi \cdot k_C (d - d_0)(1-\nu^2)/(2E \cdot \tan(\alpha))}$. The opening angle ($\alpha$) of the AFM tips was 35°, the Poisson ratio was set to $\nu = 0.5$, the value for incompressible material. E was then determined by a least square fit (fit-range: 10–40 nm indentation), as described by the Radmacher group [33, 34] using Igor Pro data analysis software (Wavemetrics, Lake Oswego, USA).

Cytochemistry

HMSC, hOB and MG63 cells were grown on non- or collagen I-coated glass slides (polystyrene slides were not used because of autofluorescence < 485 nm). The cells were fixed with 4% paraformaldehyde, permeabilized with 0.2%

Triton X-100 and blocked with 3% BSA. Prior to blocking, Image-iT^{TM} FX signal enhancer (Molecular Probes, Invitrogen) was applied on the slides. Primary antibodies for osteocalcin (Santa Cruz, USA), ErbB2 (Abcam, Cambridge, UK), and paxillin (Epitomics, Burlingame, USA) were applied overnight at 4°C. The following conjugated secondary anti-rabbit antibodies were used: Alexa Flour 488 or Alexa Flour 594 (Molecular probes) and Rhodamine Red (Dianova, Hamburg, Germany). Paxillin immuno-detection was combined with the cytoskeleton dye – phalloidin, conjugated to Alexa Flour 546 (Molecular probes). DAPI (4´,6-Diamidino-2-phenylindol, Molecular probes) was used for nuclear labeling in all of the stainings. HMSCs were differentiated into OBs and stained with von Kossa as described in Bocker *et al.* [37]. Alkaline posphatase (Sigma-Aldrich), senescent cell staining (Sigma-Aldrich) and *in situ* cell death detection (TUNEL technology) kits (Roche, Penzebrg, Germany) were used according to the supplier's recommendations. All types of stainings were independently performed at least twice. Photomicrographs were taken with the Axiocam MRm or Axiocam ICc3 camera (Carl Zeiss) on an Axioskope 2 microscope (Carl Zeiss).

Confocal microscopy

Confocal laser scanning microscope (LSM510, Carl Zeiss) was used to obtain confocal photomicrographs of paxillin and phalloidin co-stainings. The argon (488 nm) and helium/neon (543 nm) lasers were consecutively used. The emitted signals were collected with a 63x objective and images (1024 x 1024 pixels^2) were taken throughout the 'equator' of the cells. Large cells were scanned at several positions and the images were subsequently merged to obtain high-resolution view of the entire cells.

Calculation of focal adhesion area

The confocal microscopy images of paxillin-labelled hMSC, hOB and MG63 cells were further processed using the Image-Pro Plus program version 4 (Media Cybernetics, Bethesda, USA). Firstly, total cell area was measured; and secondly, the paxillin-occupied area was automatically calculated by setting a threshold level. The threshold level of 0.5 μm^2 was selected as a minimal focal adhesion area based on Franz *et al.* [38]. The focal adhesion area was thereby estimated as a percentage of the total cell area and it was averaged from 12 cells in two independent stainings.

Cell adhesion assay

Cell adhesion assays were performed on collagen I-coated 96-well plates (Nunc). After coating, the plates were rinsed and blocked with 5% skim milk powder (Merck, Darmstadt, Germany) in PBS with 0.2% Tween 20 for 30 min. HMSCs, hOBs and MG63 cells were plated in triplicates (3000 cells/well) and incubated for 30 min at 37°C. Non-adherent cells were removed by washing with PBS. Cell adhesion was estimated using a colorimetric method, based on a NPAG (p-nitrophenyl N-acetyl-beta-D-glucosaminide, Sigma-Aldrich) reaction. Absorbance was measured at 405 nm by microtitre-plate reader (Microtek Laborsysteme GmbH, Overath, Germany). Control wells, coated with just the blocking solution were used to subtract the background adhesion for each cell type. The percentage of adherent cells was finally calculated as suspensions of 3000 cells were used for maximal references. Two independent experiments were performed.

Statistical analysis

Quantitative data were processed with SigmaPlot version 8. Means and standard deviations are illustrated in the figures. Statistical analyses were performed using SigmaStat version 3 (Systat Software GmbH, Erkrath, Germany). Pairwise significances were calculated using the Student's t-test while for multiple comparisons Dunn's or Duncan's tests were used. A value of $P < 0.05$ was considered significant.

Results

HMSC-, hOB- and MG63-specific features and growth in culture

HMSC, hOB and MG63 cells were expanded in polystyrene T-75 flasks and the cultures were frequently monitored for their morphological appearance. As reported by previous investigators [6–9], hMSC cultures contain both, spindle-shaped RS cells and large FC cells (Fig. 1A). HOBs exhibited their typical polygonal, flattened morphology (Fig. 1C) [39, 40] whereas attached MG63 cells revealed an oval to spindle-shaped appearance (Fig. 1E) [16].

Next we performed three staining protocols to check for typical features of the analyzed cells. HMSCs were grown in osteogenic media for 21 days and the deposited mineralized matrix was positively stained with von Kossa (Fig. 1B). HOBs showed a strong cytosolic signal for the bone marker protein, osteocalcin (Fig. 1D) and MG63 cells were positive for ErbB2, a previously reported marker for metastatic osteosarcoma cells (Fig. 1F) [41].

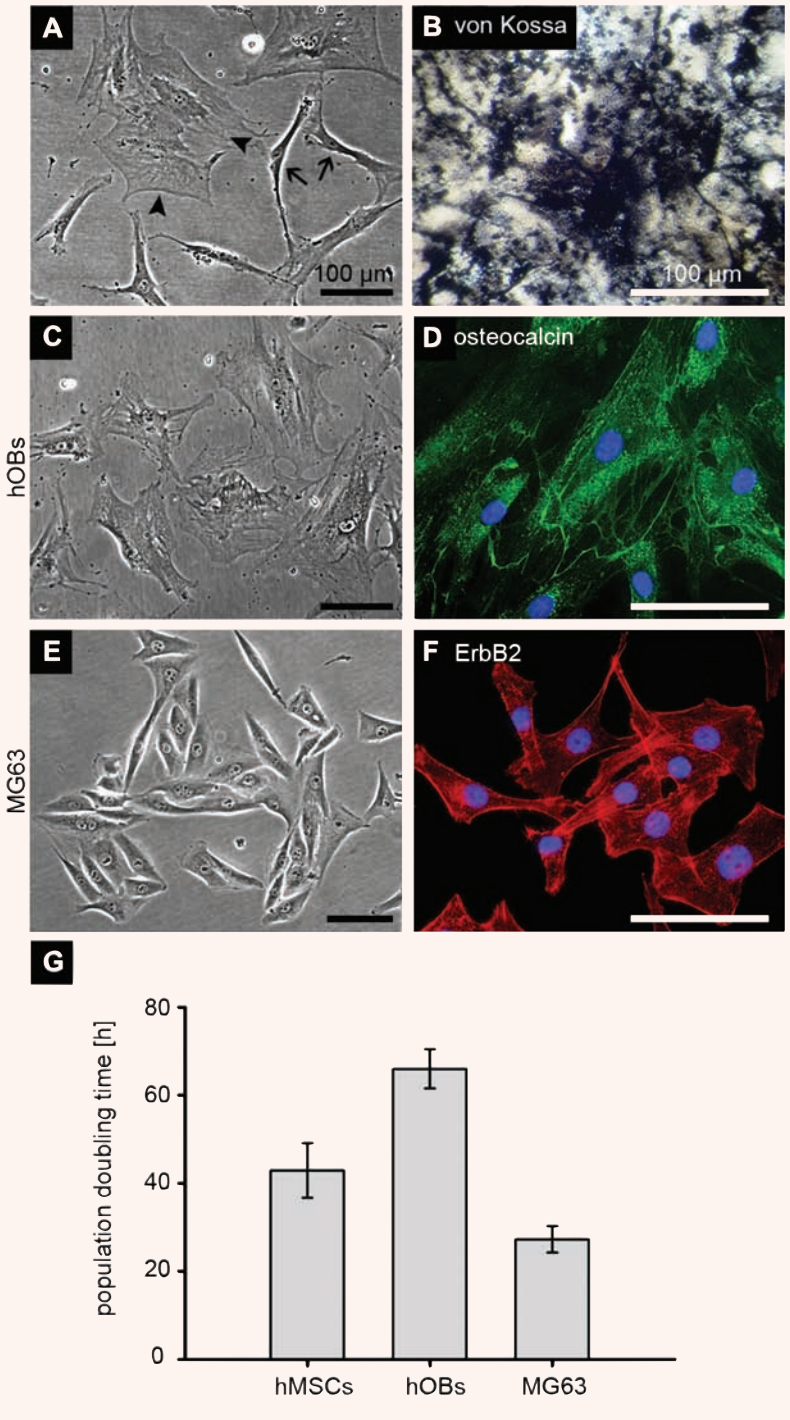

Fig. 1 Cell culture appearances and specific features of hMSC, hOB and MG63 cells. Phase-contrast images of hMSC (**A**), hOB (**C**) and MG63 (**E**) cells. HMSC culture contained two distinct subpopulations: small, spindle-shaped RS cells (arrows) and large, flat FC cells (arrow heads). HOBs exhibited their typical polygonal and flattened morphology in contrast to MG63 cells, which revealed a variety of appearances, from oval and triangular to spindle-shaped. Each of the cell types possessed specific characteristics: hMSCs differentiated into OBs after 21 days and stained positive for von Kossa (**B**); hOBs showed expression of the bone marker protein, osteocalcin (**D**) and ErbB2, an osteosarcoma-related gene, gave a strong signal in MG63 cells (**F**). In addition, there were clear differences in the PD time of the analysed cell types (average of three passages) (**G**). Bars: 100 µm.

We looked at the growth characteristics of the three cell types (Fig. 1G). As expected MG63 cells proliferated at the fastest rate. HOBs proliferated the slowest while hMSCs (mixture of RS and FC cells) proliferated at an intermediate rate. Furthermore we segregated hMSCs to RS and FC cells and monitored

the growth of single-cell derived clones. RS and FC cell clones were grown in culture for 35 days and the total number of RS cells was 5.3-fold higher then FC cells (Supplementary Fig. S1A). The PD time of RS cells was significantly higher then that recorded for FC cells (Supplementary Fig. S1B).

Next, in order to exclude the possibility that FC cells constitute senescent or pre-apoptotic cells in the hMSC culture we performed apoptosis (TUNEL) and senescent (β-galactosidase) assays (Fig. 2 A–C). We included for each assay a positive control: hMSCs treated with DNase I to mimic apoptosis and hMSCs exposed for 24 hrs to 2 mM hydroxyurea, an agent known to induce cellular senescence [42]. We did not detect apoptotic or senescent FC cells in the passages used in this study. In contrast, the parallel controls stained positive in both assays. Finally, since FC and hOB cells looked alike we preformed a histochemical test for alkaline phosphatase activity. Indeed, a large portion of FC cells showed active alkaline phosphatase (Fig. 2D), an observation correlating well with the study of Colter *et al.* [8].

Topography and surface roughness of the substrates

We cultured hMSC, hOB and MG63 cells on three different substrates – polystyrene, glass and collagen I-coated glass. The AFM images of polystyrene slides showed typical fibrous-like topography due to the polymeric form of this material and had the highest mean roughness of 2.9 ± 2.1 nm. The surface of the glass slides was granular and slightly rough (mean roughness of 0.8 ± 0.2 nm), while coating with collagen I led to a more filamentous appearance and a 2.5-fold roughness augmentation *versus* glass (Supplementary Fig. S2).

Topography and height profiles of representative RS, FC, hOB and MG63 cells

A total of 49 cells underwent analyses of cell topography, height and morphometry. Fig. 3A and B show the AFM deflection and height images of single RS, FC, hOB and MG63 cells, respectively, on polystyrene. The deflection images, (Fig. 3A) revealed small corrugations, such as sub-membranous structures (mainly cytoskeleton). The height images (Fig. 3B) showed the overall topography and the false colours (from brown to white) reported on the cell height. Thus, the nuclear region appeared in almost white colour. Furthermore, from the height images precise information about the x-y-plane deviations of any cellular part could be extracted and hereby a height profile along any inserted line could be obtained (white lines in Fig. 3B and corresponding profiles in Fig. 3C). Taken together, the height of the nuclear region was comparable in both, FC and hOB cells, while the height of RS cells was 2-fold lower then MG63 cells. Interestingly, when cells were grown on the other two substrates, non- or collagen I-coated glass slides, their height was altered. The most pronounced changes in height were observed for RS and MG63 cells. Their height increased on non-coated glass (with 1.4- and 1.2-fold, respectively) and particularly for MG63 cells it decreased 1.7-fold on collagen I *versus* polystyrene (Supplementary Fig. S3).

Finally, due to the high scanning resolution of the AFM images we obtained 5-fold zoomed pictures allowing the clear visualization of actin stress fibers, which lay closely under the plasmalemma (Fig. 3D). Interestingly, FC and hOB cells revealed a ruffled topography and very similar, thicker stress fibers. The latter were also distinguishable in the height profile (Fig. 3C), where each of the small peaks indicates underlying actin bundles. RS cells had much thinner actin filaments and numerous filopodia. Additionally, some actin accumulations could be noticed in lamellipodia. In contrast to all, MG63 cells exhibited very smooth surfaces and almost no stress fibers.

Cell morphometry

Cell area and volume were calculated from the AFM height images (Supplementary Table S1). From these calculations, we determined that RS, FC, hOB and MG63 cells had very distinct morphometric features and when distributed by area and volume on polystyrene, these cells occupied unique ‘niches’ (Fig. 4A). MG63 cells were the smallest in area followed RS cells. FC and hOB domains were located close to each other. However, the hOBs displayed areas and volumes, 1.7- and 1.9-fold, bigger then those of FC cells. The volume of the RS, FC and MG63 cells was in a similar range (Supplementary Table S1). Furthermore, the cell area and the volume were

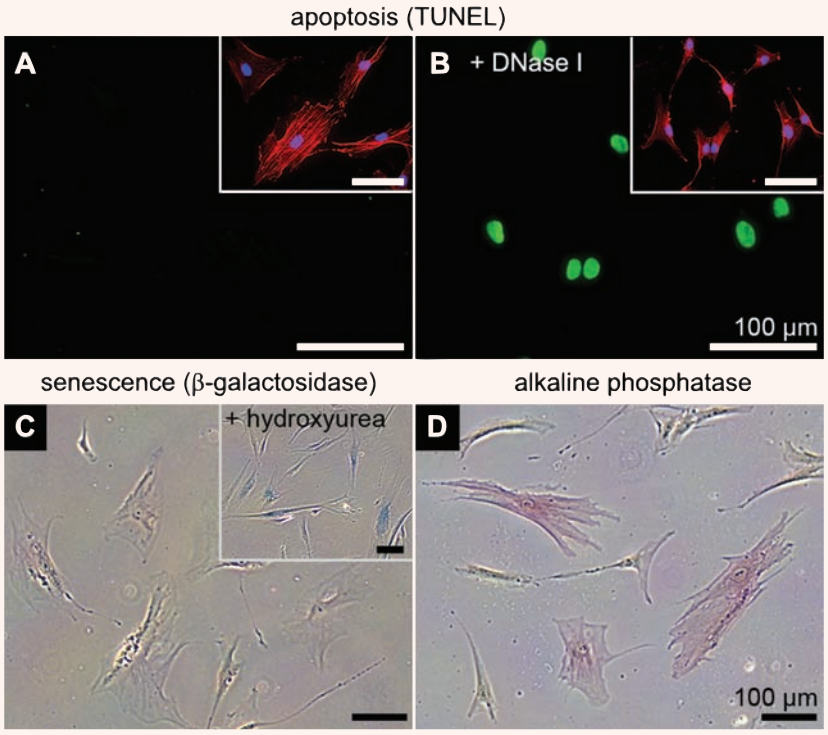

Fig. 2 FC cell characterization. (**A**) Apoptosis detection at single cell level based on labeling of DNA strand breaks (TUNEL technology). No positive FC cells were observed. (**B**) Control of the TUNEL assay, hMSCs exposed to DNase I, in which every nucleus is positively marked. Insets in (A) and (B) show corresponding cytoskeletal and nuclear stainings to demonstrate the cell availability. Furthermore, FC cells did not exhibit β-galactosidase activity, an attribute of senescence (**C**). Inset in (**C**) presents hydroxyurea-treated hMSCs as a positive control. Several of these cells are senescent (blue labeling). (**D**) Cytochemical enzyme test for alkaline phosphatase. Many FC cells revealed alkaline phosphatase activity (stained in red violet). Bars: 100 µm.

influenced by the other two substrates (glass and collagen I) (Supplementary Table S1). For example, MG63 cells showed an intriguing alteration on collagen I where they revealed a 1.7-fold increase in cell area, but a 1.5-fold decrease in cell volume in comparison to the polystyrene substrate.

Next, we calculated ellipse and flatness shape factors. We observed, for each cell type, non-significant variations of the ellipse shape factor with regards to the different substrates (Fig. 4B). However, it was obvious that RS cells had the highest ellipse shape factor, defining these cells as the most oblong cell type.

The results for the flatness shape factor are shown in Fig. 4C. RS cells demonstrated similar flatness on the fibrous substrates, whereas their flatness significantly reduced on glass. MG63 cells had the most elevated shape factor on glass, but interestingly, they appeared also much rounder on polystyrene. Moreover, on these two substrates MG63 cells were also significantly more round than RS cells (RS *versus* MG63 on polystyrene $P = 0.00002$, RS *versus* MG63 on glass $P = 0.0041$). In contrast, when MG63 were grown on collagen I, a significant change towards a 2.3-fold augmented flatness shape factor was observed. FC and hOB cells grouped again together, as they had the lowest and very similar flatness shape factors on the three different substrates, and in comparison to RS and MG63 cells, they were indeed significantly flatter.

Cytoskeleton organization and extent of adhesion

We performed F-actin (phalloidin) and focal adhesion (paxillin) stainings for each cell type on collagen I (Fig. 5A and B). RS cells portrayed their typical spindle-shaped morphology, and the majority of actin fibers ran in parallel to the cell axis. In addition, wave-like actin accumulations were located at the stretched lamellipodia, a finding already observed in the AFM images (Fig. 5A and Fig. 3D). FC cells and hOBs had a very distinguishable actin cytoskeleton organization – much more robust, with a great amount of criss-crossing actin filaments and larger, bulky stress fibers (Fig. 5A and Fig. 3D). Conversely, MG63 cells had almost no pronounced stress fibers, and most of the actin was organized as a cortical ring (Fig. 5A).

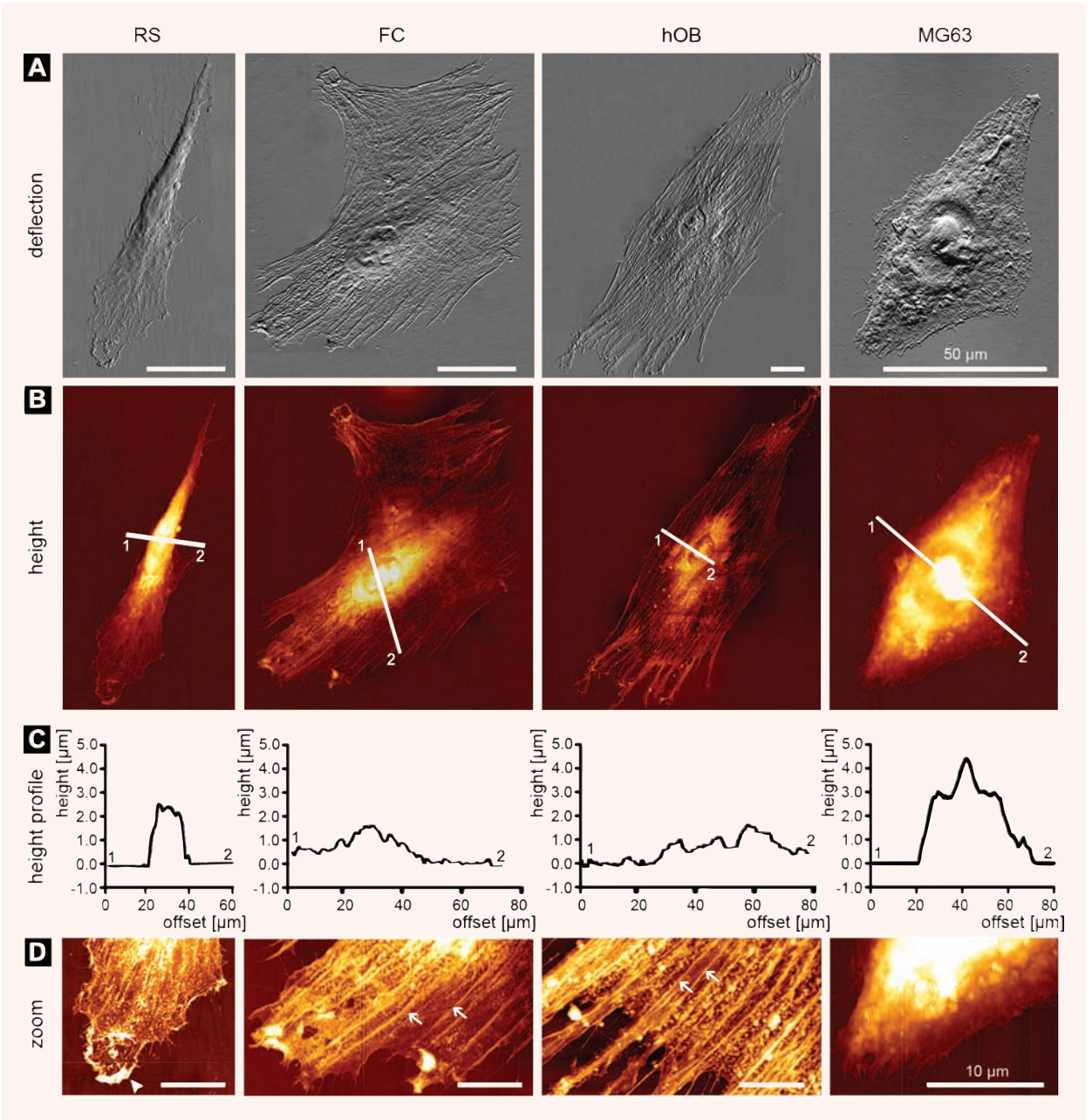

Fig. 3 Topography and height profile of the analysed cell types. AFM deflection images (**A**) of a single RS, FC, hOB and MG63 cells on polystyrene. The small corrugations reflected submembranous structures. AFM height images of the above cells are shown in (**B**). The colour scale indicates the height of a particular cell region. From these images a height profile could be extracted for any inserted line. Examples are shown in (**C**), where the height profiles along the white lines in (**B**) are shown. The nuclear region was used for comparing the heights between the cell types. We found that the MG63 cells had the highest nuclear regions, followed by RS cells, while FC and hOB cells showed similar, lower heights. Details about the actin cytoskeletal organization were revealed in zoomed images (**D**). RS cells had thin actin filaments and some actin accumulations (arrow head) in lamellipodia, as well as numerous filopodia. FC and hOB cells showed ruffled topographies and very similar, thicker stress fibers (arrows). MG63 cells exhibited a very smooth surface and almost no stress fibers. Bars: (**A**) 50 µm; (**D**) 10 µm.

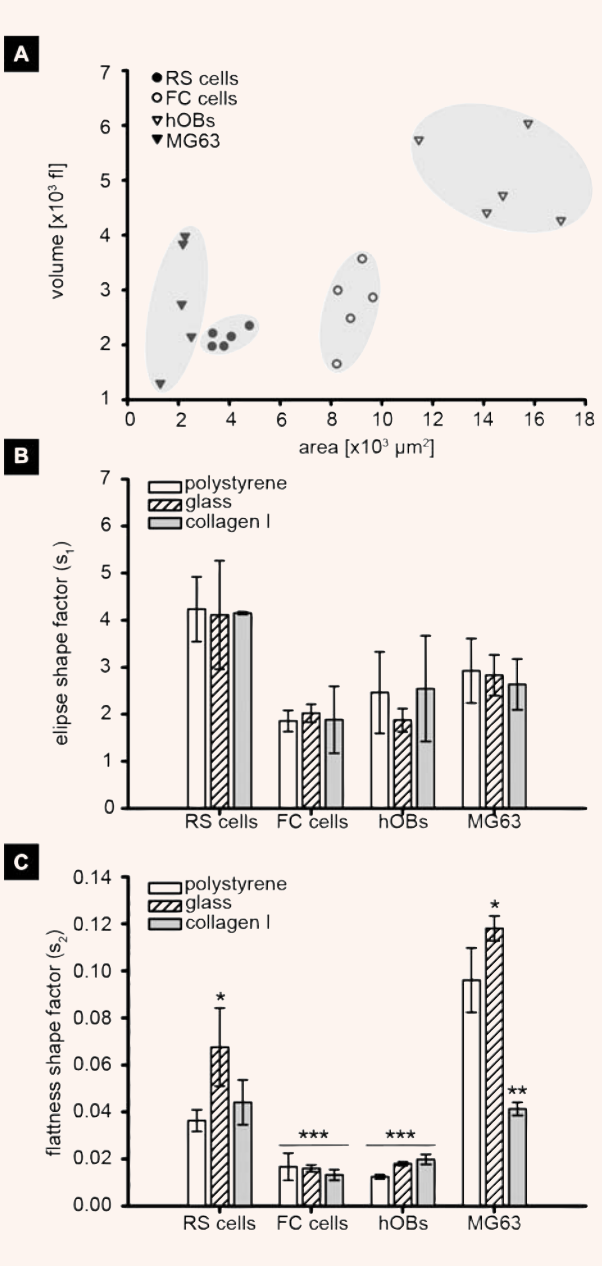

Fig. 4 Morphometric analysis of RS, FC, hOB and MG63 cells (42 cells in total). (**A**) Scatter plot of cell area and volume on polystyrene. HOBs were the most outstanding cell type due to their large area and volume values. Furthermore, in order to confirm that representative cells were used in the analyses, we calculated ellipse shape factors (**B**) ($s_1 = 1$ corresponds to a disk-shaped cell and $s_1 \rightarrow \infty$ to an oblong one). RS cells were the most oblong cell type. With regard to the three different substrates, non-significant variations of s1 were observed for each cell type ($P \geq 0.4$). The flatness shape factor analyses (**C**) ($s_2 = 0$ corresponds to flat disk and $s_2 = 1$ to a sphere-like ellipsoid) demonstrated that FC and hOBs cells have similar and significantly pronounced flatness independently of the substrates (***FC or hOB on all substrates *versus* RS polystyrene, $P < 0.05$). In contrast, RS and MG63 cells behaved differently on the substrates. Both cell types became significantly more round on glass (*RS on glass *versus* polystyrene, $P = 0.0047$ and *MG63 on glass *versus* polystyrene, $P = 0.0409$) and particularly for MG63 cells a very pronounced change towards enhanced flatness was observed on collagen I (**collagen I *versus* polystyrene, $P = 0.0006$).

With regards to focal adhesions, we quantified the percentage of paxillin-positive areas and performed adhesion assays on collagen I. We used young and older hMSC passages in order to discriminate between RS and FC cell adhesion, respectively. Thus we found that the focal adhesions occupied around 4–9% from the FC and hOB cell terrains (Fig. 5C) and thereof these cells had significantly (1.4-fold) stronger adhesion to collagen I in comparison to RS and MG63 cells (Fig. 5D).

Force mapping and elasticity measurements

To characterize the elasticity of the cells, mean Young's modules were calculated. The only values taken, were these calculated from force curves that were recorded in the nuclear and peri-nuclear region (schematic model in Fig. 6A and example force curves in Fig. 6B). The mean Young's modules of all analyzed cells are shown in Figure 6C. We could not detect a cell-type specific Young's modulus in the region where the measurements were taken. In broad outline, RS, FC and hOB cells showed comparable stiffness on the three different substrates. A slight substrate-related tendency towards an increase of elasticity (decrease of the Young's modulus) on glass was observed for RS and hOB cells. MG63 cells again demonstrated a collagen I-specific response, as in addition to the increased area and flatness (Supplementary Table S1 and Fig. 4C), they showed a significantly (2-fold) lower Young's modules (*versus* polystyrene), corresponding to a decrease in stiffness.

Discussion

In the present study we have compared the morphometric and elastic features of two hMSC subtypes, hOBs and osteosarcoma cells. We analyzed the above cells on three different substrates – polystyrene, glass and collagen I. These substrates were selected due to the following reasons: polystyrene is the usual material used for cell expansion of adherent cells; glass is frequently employed in microscopic and histological cell analyses; and collagen I resembles a natural substrate since collagen is the most abundant organic molecule in bone.

We started with concise analyses on the cell morphology, growth and molecular hallmarks. We observed RS and FC cells in hMSC cultures [8, 9]. What is more, the RS cell phenotype we detected showed greater likeness to the so called 'RS-1C' cell variant that is defined as wider, spindle-shaped cells which appear in the initial culture approximately at the 10^{th} day [9]. We supposed that we had a high incidence of this variant because our cultures were passaged several times. HMSC, hOB and MG63 cells had different proliferation activities and the calculated PD times are comparable with those found by others in the field [16, 43, 44]. With regards to RS and FC cells, we agree with observations by Sekiya *et al.* [9], who showed that the portion of RS cells in the mixed hMSC culture decreased over time. In contrast, the culture in higher passages was predominantly composed of FC cells. Therefore in some of our experiments we used young and old passages in order to enrich for either RS or FC cells. Additionally, our histochemical analyses showed that FC cells were not senescent or apoptotic in the passages used here, but that some exhibited alkaline phosphatase activity. In this connection, it is noteworthy to mention the previous finding of Colter *et al.* who report that the increase in the FC portion of the culture was accompanied by an increase in alkaline phosphatase [8]. However, previous analyses from both our and the Prockop groups have shown that FC cells still present a panel of surface epitopes which are considered as MSC criteria [8, 18]. Finally, hMSCs successfully differentiated in the osteogenic lineage and hOBs and MG63 have retained their osteocalcin and ErbB2 expression, respectively.

Next, we precisely investigated the morphometric characteristics of RS, FC, hOB and MG63 cells. AFM images of MG63 and other osteoblasts-like cell lines (MC3T3, Saos2) have already been published [33, 45, 46]. To date, there are two AFM studies dealing with hMSCs, but the authors looked for changes in the topography and elasticity of hMSCs during differentiation [47, 48]. Here, however, we show for first time AFM images of single RS, FC and hOB cells. Interestingly, a topographical similarity between FC and hOB cells could be discerned easily from the images, whereas RS and MG63 cells had very distinguishable features. Then the estimation of the ellipse shape factor was very useful to prove that we picked relatively representative cells for each type, since we selected each cell by its morphology. On the other hand, the flatness shape factor, as a three-dimensional measure, could indicate how the selected substrates influence cell spreading. RS and MG63 cells became round on glass, whereas FC and hOB cells had very similar, much lower flatness shape factors. Moreover, their flatness almost did not change with respect to the different substrates. This finding suggested that among the analyzed cell types, cells with very big areas and volumes were less sensitive to variations in substrate roughness.

The apparent differences in flatness between RS, FC, hOB and MG63 cells might be related to cell-specific strength of adhesion and properties of the actin cytoskeleton. Indeed, RS and MG63 cells presented a very low content of focal adhesions. In FC and hOB cells, the focal adhesions occupied up to 9% of the cell terrain and these cells had significantly stronger adhesion to collagen I. Moreover, FC and hOB cells contained some centrally localized focal adhesions, which show similarity to the so called 'mature or fibrillar adhesions'. These adhesions are found in less motile cells, and are accountable for more firm adhesion to the matrix [49].

Furthermore, FC and hOB cells exhibited a high content of robust stress fibers, while RS cells had a more refined actin architecture and many wave-like actin accumulations. Importantly, Yourek *et al.* [48] have reported that upon osteogenic differentiation, the actin cytoskeleton of hMSCs rearranges into a more vigorous, crisscrossed pattern. In contrast, MG63 cells organized the actin in a cortical ring.

The actin architecture has great impact not only on cell morphology and behaviour but also on cell biophysical attributes. The effect of actin organization on cell stiffness has been already attested as it has been observed that a cell becomes more elastic upon chemical disruption of its actin stress fibres [46,

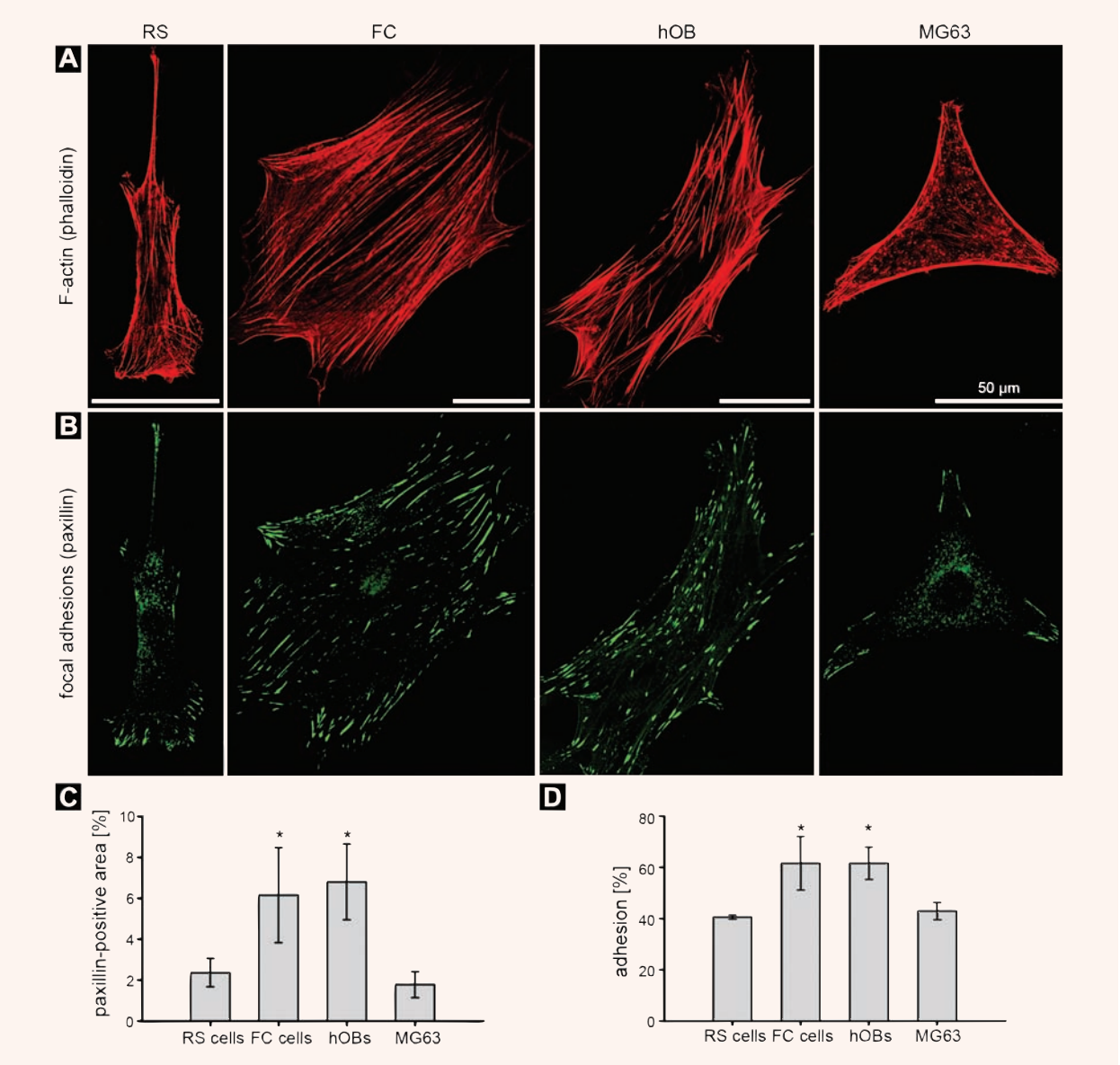

Fig. 5 Cell adhesion and cytoskeleton characterization. Focal adhesions and F-actin of the analysed cells were visualized by phalloidin and paxillin co-staining, respectively, on collagen I slides (**A** and **B**). FC and hOB cells exhibited similar actin architectures, consisting of bulky stress fibers strained between numerous, large focal adhesions. Conversely, RS and MG63 cells showed small and sparse focal adhesions as well as thin and less abundant stress fibers. Quantification of paxillin-positive areas, as a measure of the content of focal adhesions (**C**) (12 samples for each cell type), correlated well with the functional adhesion assays, in which the cells were allowed to attach to collagen I for 30 min (**D**) (a representative experiment with triplicates). Thus, we found that FC and hOB cells had similar and significantly higher extent of adhesion compared to RS and MG63 cells (* FC or hOB *versus* RS or MG63, $P < 0.05$). Bars: 50 µm.

50]. AFM elasticity measurements have been already performed on many different cell types. In Fig. 7 we reviewed several such examples but also others linked to the bone field. Our results were comparable with the Young's modules of fibroblastic cells. However, with regards to hMSCs a recent study by Yourek *et al.* [48] reported the stiffness of non- and differentiated hMSCs in the much higher range of

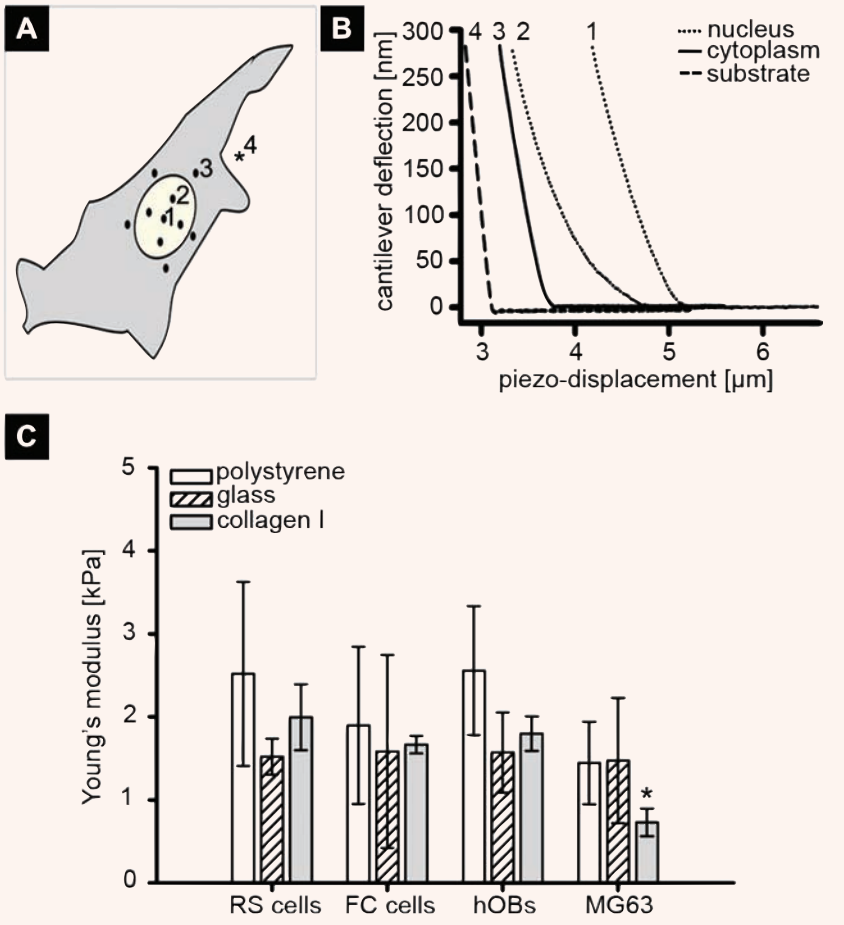

Fig. 6 Cell elasticity measurements. The mean Young's modulus of each cell was calculated from 20 force curves, taken at 10 different points in the nuclear and peri-nuclear region (**A**). Each curve represents the average cantilever deflection of approach and retract cycle. Example force curves are shown in (**B**), where curves 1–3 were recorded within the cell body and correspond to points 1–3 in (**A**). Curve 4 indicates the measurement of the substrate (marked with a star in (A)). The cantilever force constant for all four curves was 27 mN/m. The Young's modules of all analysed cells (56 cells in total) fell in the range between 0.7 ± 0.1 and 2.6 ± 0.7 kPa (**C**). RS, FC and hOB cells showed comparable stiffness on the three different substrates. Intriguingly, MG63 cells demonstrated a collagen I-specific response, as they showed a 2-fold significantly lower Young's modules, corresponding to increased elasticity (*collagen I *versus* polystyrene, $P = 0.0183$).

33–53 kPa. Possible explanations for these differences are that firstly, Yourek *et al.* [48] used the original Hertz model [35], which describes an indenting sphere, rather than an indenting cone. This model is only suitable as long as the indentation is smaller than the radius of the sphere, if not the Young's modulus will be overestimated. Secondly, the authors performed force curve arrays (32 x 32 force curves) and randomly selected three curves per cell to calculate the Young's modulus. We intentionally measured the Young's modulus in the nuclear region, in order to exclude any artificially high values arising from compressing the soft cell sample and consecutively sensing the stiff substrate [59]. Nevertheless, performing well-controlled force curve arrays can provide an overview of the elasticity of different regions of an entire cell. Therefore, in future studies, such arrays should be recorded for the four cell types investigated here, especially because, while looking solely at the nuclear region, we have observed only small cell-specific or substrate-related variations in Young's modules. An exception was the behaviour of MG63 cells on collagen I. On this substrate we saw significant changes in cell spreading and elasticity and thus far, only these cells demonstrated cell-specific Young's modulus. In general, upon cell flattening, the actin density and the intracellular tension increase, and hereby the cell stiffens. However, results from shape-engineered fibroblasts proposed that, apart from actin, several other mechanistic factors, such as membrane and nucleus bending properties, can also act on the overall cell elasticity [60]. Furthermore, molecular analysis of cells cultured on collagen I gels indicated that the substrate rigidity itself can directly regulate focal adhesions and intracellular tension [61]. Lastly, a recent study from Darling *et al.* [62] has investigated chondrosarcoma

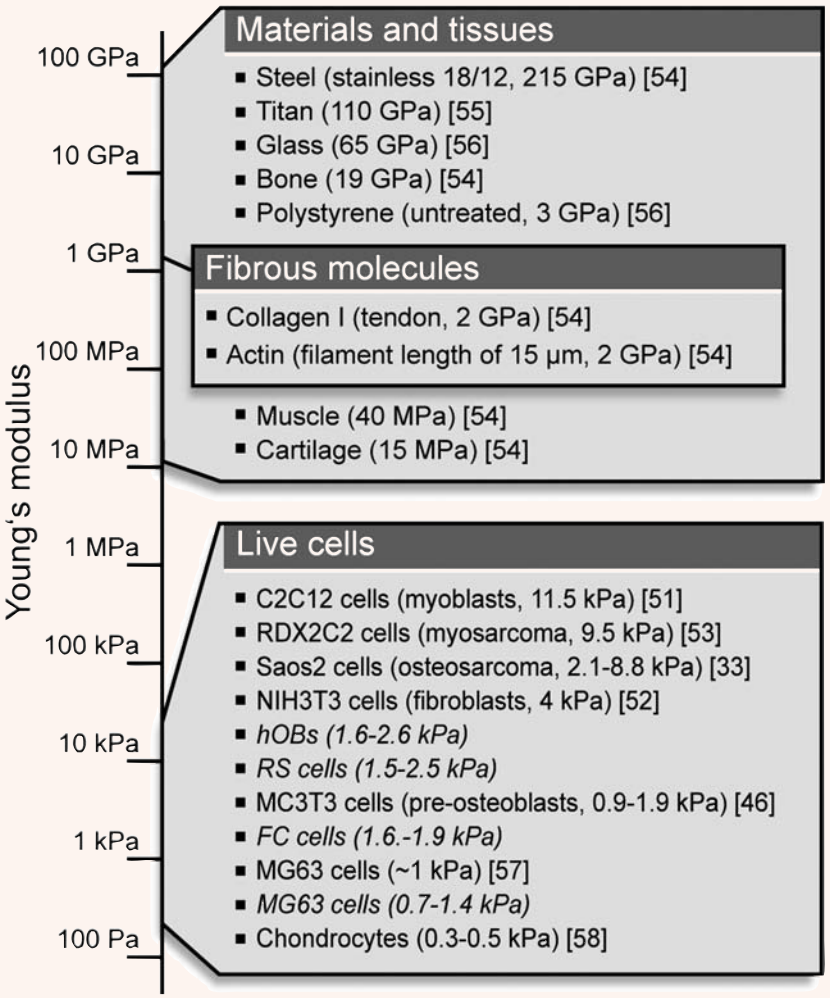

Fig. 7 Overview of the Young's modulus of different samples related to the bone field and our study. For instance, shown are measurements of cortical bone, stainless steel and titan (materials used for hip prostheses); collagen I and different cell types. Our data fitted in the range of the Young's modulus values for fibroblast-like cells, but also showed new lineaments for the cells analysed here. The measurements for RS, FC, hOB and MG63 cells are in italic font and the range of the values corresponds to the measurements taken on the three different substrates.

cell lines and suggested that a decrease in cell viscosity can be associated with tumour transformation. With respect to MG63 cells and their intriguing response to collagen I, it is still unknown whether this response is a tumor-related feature. Additionally, the underlying molecular mechanisms remain to be determined.

In summary, our study showed novel morphometric, adhesion and biophysical features of hMSC, hOB and MG63 cells. We correlated the cell-specific flatness factors to the amount of focal adhesions. Thus, we found that the FC subtype of hMSCs has very similar characteristics to hOBs, which strengthen the idea that FC cells resemble pre-OBs in primary hMSC cultures. Finally, an improved understanding of the physical characteristics of different cell types and their nano-mechanical changes upon different stimuli may not just lead to a more profound knowledge about 'the cell', but it may also aid in the development of new, effective approaches for tissue engineering or inhibiting metastasis by controlling or reinforcing the structure of the cell.

Acknowledgements

Denitsa Docheva was supported by the AO Research Fund of the AO Foundation (grant 05-D83). Cvetan Popov was supported by the Bavarian Research Foundation (grant DPA-51/05), Daniela Padula and Hauke

Table S1: Area and volume of RS, FC, hOB and MG63 cell on three different substrates

Cell types	Average cell area [μm^2]			Average cell volume [fl]		
	polystyrene	glass	collagen I	polystyrene	glass	collagen I
RS cells	3866.4±541.3	2144.2±384.2	2256.5±289.2	2132.3±143.3	1695.1±319.5	1196.4±70.1
FC cells	8824.0±548.2	12212.3±2448.7	11891.9±704.3	2710.9±634.0	6302.5±1983	3482.2±1255.0
hOBs	14616.3±1864.7	9880.8±67.9	13189.3±2413.9	5034.2±716.6	4393.4±820.5	5353.4±866.9
MG63	2068.3±411.5	1782.3±215.1	3537.5±192.8	2801.4±1013.1	2753.4±522.1	1901.7±92.1

Clausen-Schaumann gratefully acknowledge financial support of the German Excellence Initiative *via* the 'Nanosystems Initiative Munich (NIM)'. We also acknowledge Thomas Möllenhoff for programming parts of the image analysis software, Robert Brunner and JPK Instruments for technical assistance, Matthias Wierer for von Kossa staining of differentiated MSCs, Ines Westphal for confocal microscope assistance and Edward Fellows for carefully reading the manuscript.

Supplementary Material

The following supplementary material is available for this article:
Fig. S1 Growth characteristics of RS and FC cells.
Fig. S2 Topography and mean roughness of the different substrates.
Fig. S3 Height analysis of RS, FC, hOB and MG63 cells.
Table S1. Area and volume of RS, FC, hOB and MG63 cell on three different substrates.

This material is available as part of the online article from: http://www.blackwell-synergy.com/doi/abs/10.1111/j. 1582-4934. 2007.00138.x
(This link will take you to the article abstract).

Please note: Blackwell Publishing are not responsible for the content or functionality of any supplementary materials supplied by the authors. Any queries (other than missing material) should be directed to the corresponding author for the article.

References

1. **Blonder J, Xiao Z, Veenstra TD.** Proteomic profiling of differentiating osteoblasts. *Expert Rev Proteomics.* 2006; 3: 483–96.
2. **Docheva D, Popov C, Mutschler W, Schieker M.** Human mesenchymal stem cells in contact with their environment: surface characteristics and the integrin system. *J Cell Mol Med.* 2007; 11: 21–38.
3. **Krampera M, Pizzolo G, Aprili G, Franchini M.** Mesenchymal stem cells for bone, cartilage, tendon and skeletal muscle repair. *Bone.* 2006; 39: 678–83.
4. **Schieker M, Seitz H, Dorsse I, Seitz S, Mutschler W.** Biomaterials as scaffold for bone tissue engineering. *Eur J Trauma.* 2006; 32: 114–24.
5. **Baksh D, Song L, Tuan RS.** Adult mesenchymal stem cells: characterization, differentiation, and application in cell and gene therapy. *J Cell Mol Med.* 2004; 8: 301–16.
6. **Digirolamo CM, Stokes D, Colter D, Phinney DG, Class R, Prockop DJ.** Propagation and senescence of human marrow stromal cells in culture: a simple colony-forming assay identifies samples with the greatest potential to propagate and differentiate. *Br J Haematol.* 1999; 107: 275–81.
7. **Colter DC, Class R, Digirolamo CM, Prockop DJ.** Rapid expansion of recycling stem cells in cultures of plastic-adherent cells from human bone marrow. *Proc Natl Acad Sci USA.* 2000; 97: 3213–8.
8. **Colter DC, Sekiya I, Prockop DJ.** Identification of a subpopulation of rapidly self-renewing and multipotential adult stem cells in colonies of human marrow stromal cells. *Proc Natl Acad Sci USA.* 2001; 98: 7841–5.
9. **Sekiya I, Larson BL, Smith JR, Pochampally R, Cui JG, Prockop DJ.** Expansion of human adult stem cells from bone marrow stroma: conditions that maximize the yields of early progenitors and evaluate their quality. *Stem Cells.* 2002; 20: 530–41.
10. **Smith JR, Pochampally R, Perry A, Hsu SC, Prockop DJ.** Isolation of a highly clonogenic and multipotential subfraction of adult stem cells from bone marrow stroma. *Stem Cells.* 2004; 22: 823–31.
11. **Prockop DJ, Sekiya I, Colter DC.** Isolation and characterization of rapidly self-renewing stem cells from cultures of human marrow stromal cells. *Cytotherapy.* 2001; 3: 393–6.

12. **Tataria M, Quarto N, Longaker MT, Sylvester KG.** Absence of the p53 tumor suppressor gene promotes osteogenesis in mesenchymal stem cells. *J Pediatr Surg.* 2006; 41: 624–32.
13. **Tolar J, Nauta AJ, Osborn MJ, Panoskaltsis MA, McElmurry RT, Bell S, Xia L, Zhou N, Riddle M, Schroeder TM, Westendorf JJ, McIvor RS, Hogendoorn PC, Szuhai K, Oseth L, Hirsch B, Yant SR, Kay MA, Peister A, Prockop DJ, Fibbe WE, Blazar BR.** Sarcoma derived from cultured mesenchymal stem cells. *Stem Cells.* 2007; 25: 371–9.
14. **Dorfman HD and Czerniak B.** Bone cancers. *Cancer.* 1995; 75: 203–10.
15. **Cohen MM, Jr.** The new bone biology: pathologic, molecular, and clinical correlates. *Am J Med Genet A.* 2006; 140: 2646–706.
16. **Pautke C, Schieker M, Tischer T, Kolk A, Neth P, Mutschler W, Milz S.** Characterization of osteosarcoma cell lines MG-63, Saos-2 and U-2 OS in comparison to human osteoblasts. *Anticancer Res.* 2004; 24: 3743–8.
17. **Schieker M, Pautke C, Reitz K, Hemraj I, Neth P, Mutschler W, Milz S.** The use of four-colour immunofluorescence techniques to identify mesenchymal stem cells. *J Anat.* 2004; 204: 133–9.
18. **Schieker M, Pautke C, Haasters F, Schieker J, Docheva D, Bocker W, Guelkan H, Neth P, Jochum M, Mutschler W.** Human mesenchymal stem cells at the single-cell level: simultaneous seven-colour immunofluorescence. *J Anat.* 2007; 210: 592-9.
19. **Settleman J.** Tension precedes commitment-even for a stem cell. *Mol Cell.* 2004; 14: 148–50.
20. **Rodriguez JP, Gonzalez M, Rios S, Cambiazo V.** Cytoskeletal organization of human mesenchymal stem cells (MSC) changes during their osteogenic differentiation. *J Cell Biochem.* 2004; 93: 721–31.
21. **McBeath R, Pirone DM, Nelson CM, Bhadriraju K, Chen CS.** Cell shape, cytoskeletal tension, and RhoA regulate stem cell lineage commitment. *Dev Cell.* 2004; 6: 483–95.
22. **Clausen-Schaumann H, Seitz M, Krautbauer R, Gaub HE.** Force spectroscopy with single bio-molecules. *Curr Opin Chem Biol.* 2000; 4: 524–30.
23. **Engel A and Muller DJ.** Observing single biomolecules at work with the atomic force microscope. *Nat Struct Biol.* 2000; 7: 715–8.
24. **Santos NC and Castanho MA.** An overview of the biophysical applications of atomic force microscopy. *Biophys Chem.* 2004; 107: 133–49.
25. **Lu YB, Franze K, Seifert G, Steinhauser C, Kirchhoff F, Wolburg H, Guck J, Janmey P, Wei EQ, Kas J, Reichenbach A.** Viscoelastic properties of individual glial cells and neurons in the CNS. *Proc Natl Acad Sci USA.* 2006; 103: 17759–64.
26. **Costa KD.** Single-cell elastography: probing for disease with the atomic force microscope. *Dis Markers.* 2003; 19: 139–54.
27. **Matzke R, Jacobson K, Radmacher M.** Direct, high-resolution measurement of furrow stiffening during division of adherent cells. *Nat Cell Biol.* 2001; 3: 607–10.
28. **Puech PH, Poole K, Knebel D, Muller DJ.** A new technical approach to quantify cell-cell adhesion forces by AFM. *Ultramicroscopy.* 2006; 106: 637–44.
29. **Simon A and Durrieu MC.** Strategies and results of atomic force microscopy in the study of cellular adhesion. *Micron.* 2006; 37: 1–13.
30. **Huang GT, Shagramanova K, Chan SW.** Formation of odontoblast-like cells from cultured human dental pulp cells on dentin *in vitro. J Endod.* 2006; 32: 1066–73.
31. **Butt H-J and Jaschke M.** Calculation of thermal noise in atomic force microscopy. *Nanotechnology.* 1995; 6: 1–7.
32. **Burger W, Burge J.** Digitale Bildverarbeitung.*6th ed. Berlin: Springer;* 2005. pp. 429–30.
33. **Domke J, Dannohl S, Parak WJ, Muller O, Aicher WK, Radmacher M.** Substrate dependent differences in morphology and elasticity of living osteoblasts investigated by atomic force microscopy. *Colloids Surf B Biointerfaces.* 2000; 19: 367–39.
34. **Radmacher M.** Studying the mechanics of cellular processes by atomic force microscopy. *Methods Cell Biol.* 2007; 83: 347–72.
35. **Hertz H.** Uber die Beruhrung fester elastischer Korper. *J Reine Angew Mathematik.* 1882; 92: 156–71
36. **Sneddon I.** The relation between load and penetration in the axisymmetric boussinesq problem for a punch of arbitrary profile. *Int J Eng Sci.* 1965; 3: 47–57.
37. **Bocker W, Rossmann O, Docheva D, Malterer G, Mutschler W, Schieker M.** Quantitative polymerase chain reaction as a reliable method to determine functional lentiviral titer after ex vivo gene transfer in human mesenchymal stem cells. *J Gene Med.* 2007; 9: 585–95.
38. **Franz CM and Muller DJ.** Analyzing focal adhesion structure by atomic force microscopy. *J Cell Sci.* 2005; 118: 5315–23.
39. **Annaz B, Hing KA, Kayser M, Buckland T, Di Silvio L.** Porosity variation in hydroxyapatite and osteoblast morphology: a scanning electron microscopy study. *J Microsc.* 2004; 215: 100–10.
40. **Meyer U, Meyer T, Jones DB.** Attachment kinetics, proliferation rates and vinculin assembly of bovine osteoblasts cultured on different pre-coated artificial substrates. *J Mater Sci Mater Med.* 1998; 9: 301–7.
41. **Valabrega G, Fagioli F, Corso S, Madon E, Brach dP, Biasin E, Linari A, Aglietta M, Giordano S.**

ErbB2 and bone sialoprotein as markers for metastatic osteosarcoma cells. *Br J Cancer.* 2003; 88: 396–400.

42. **Yeo EJ, Hwang YC, Kang CM, Kim IH, Kim DI, Parka JS, Choy HE, Park WY, Park SC.** Senescence-like changes induced by hydroxyurea in human diploid fibroblasts. *Exp Gerontol.* 2000; 35: 553–71.
43. **Bacakova L, Stary V, Kofronova O, Lisa V.** Polishing and coating carbon fiber-reinforced carbon composites with a carbon-titanium layer enhances adhesion and growth of osteoblast-like MG63 cells and vascular smooth muscle cells *in vitro. J Biomed Mater Res.* 2001; 54: 567–78.
44. **Izadpanah R, Trygg C, Patel B, Kriedt C, Dufour J, Gimble JM, Bunnell BA.** Biologic properties of mesenchymal stem cells derived from bone marrow and adipose tissue. *J Cell Biochem.* 2006; 99: 1285–97.
45. **Andersen LK, Contera SA, Justesen J, Duch M, Hansen O, Chevallier J, Foss M, Pedersen FS, Besenbacher F.** Cell volume increase in murine MC3T3-E1 pre-osteoblasts attaching onto biocompatible tantalum observed by magnetic AC mode atomic force microscopy. *Eur Cell Mater.* 2005; 10: 61–8.
46. **Takai E, Costa KD, Shaheen A, Hung CT, Guo XE.** Osteoblast elastic modulus measured by atomic force microscopy is substrate dependent. *Ann Biomed Eng.* 2005; 33: 963–71.
47. **Danti S, D'Acunto M, Trombi L, Berrettini S, Pietrabissa A.** A micro/nanoscale surface mechanical study on morpho-functional changes in multilineage-differentiated human mesenchymal stem cells. *Macromol Biosci.* 2007; 7: 589–98.
48. **Yourek G, Hussain MA, Mao JJ.** Cytoskeletal changes of mesenchymal stem cells during differentiation. *ASAIO J.* 2007; 53: 219–28.
49. **Zamir E and Geiger B.** Molecular complexity and dynamics of cell-matrix adhesions. *J Cell Sci.* 2001; 114: 3583–90.
50. **Rotsch C and Radmacher M.** Drug-induced changes of cytoskeletal structure and mechanics in fibroblasts: an atomic force microscopy study. *Biophys J.* 2000; 78: 520–35.
51. **Collinsworth AM, Zhang S, Kraus WE, Truskey GA.** Apparent elastic modulus and hysteresis of skeletal muscle cells throughout differentiation. *Am J Physiol Cell Physiol.* 2002; 283: C1219–27.
52. **Haga H, Sasaki S, Kawabata K, Ito E, Ushiki T, Sambongi T.** Elasticity mapping of living fibroblasts by AFM and immunofluorescence observation of the cytoskeleton. *Ultramicroscopy.* 2000; 82: 253–8.
53. **Hutter JL, Chen J, Wan WK, Uniyal S, Leabu M, Chan BM.** Atomic force microscopy investigation of the dependence of cellular elastic moduli on glutaraldehyde fixation. *J Microsc.* 2005; 219: 61–8.
54. **Howard J.** Mechanics of Motor Proteins and the Cytoskeleton. Sunderland Massachusetts: *Sinauer Associates, Inc;* 2001. pp. 148.
55. **Kuchling H.** Taschenbuch der Physik. Leipzig: Fachbuchverlag im Carl Hanser Verlag; 2004. p. 625.
56. **Halliday D; Resnick R; Walker J.** Fundamentals of Physics. 6th ed. Weinheim: Wiley-VCH GmbH&Co KGaA; 2002. p. 359.
57. **Shin D, Athanasiou K.** Cytoindentation for obtaining cell biomechanical properties. *J Orthop Res.* 1999; 17: 880–90.
58. **Darling EM, Zauscher S, Guilak F.** Viscoelastic properties of zonal articular chondrocytes measured by atomic force microscopy. *Osteoarthritis Cartilage.* 2006; 14: 571–9.
59. **Domke J and Radmacher M.** Measuring the elastic properties of thin polymer films with the atomic force microscope. *Langmuir.* 1998; 14: 3320–5.
60. **Kidoaki S and Matsuda T.** Shape-engineered fibroblasts: cell elasticity and actin cytoskeletal features characterized by fluorescence and atomic force microscopy. *J Biomed Mater Res A.* 2007; 81: 803–10.
61. **Wang YK, Wang YH, Wang CZ, Sung JM, Chiu WT, Lin SH, Chang YH, Tang MJ.** Rigidity of collagen fibrils controls collagen gel-induced down-regulation of focal adhesion complex proteins mediated by alpha2beta1 integrin. *J Biol Chem.* 2003; 278: 21886–92.
62. **Darling EM, Zauscher S, Block JA, Guilak F.** A thin-layer model for viscoelastic, stress-relaxation testing of cells using atomic force microscopy: do cell properties reflect metastatic potential? *Biophys J.* 2007; 92: 1784–91.